Heat transfer detraction for conjugate effect of Joule heating and magneto-hydrodynamics on mixed convection in a lid-driven cavity along with a heated hollow circular plate

S.K. Farid[1], Uddin M. Sharif[2], M.M. Rahman[3] and Yeo Wee Ping[3]*

[1]Mirpur Girls Ideal Laboratory Institute, Mirpur-10, Dhaka-1216, Bangladesh
[2]Department of Mathematics, Jahangirnagar University, Savar, Dhaka, Bangladesh
[3]Mathematical and Computing Sciences Group, Faculty of Science, Universiti Brunei Darussalam, Jalan Tungku Link, Gadong, BE 1410, Brunei Darussalam

**corresponding author email: mustafizur.rahman@ubd.edu.bn*

Abstract

In this paper, the influence of Joule heating and magneto-hydrodynamics on mixed convection in a lid-driven cavity along with a heated hollow circular plate placed at the centre of the square cavity is investigated. The governing equations which are derived by considering the effects of both Joule heating and magneto-hydrodynamics are solved via the penalty finite-element method with the Galerkin-weighted residual technique. The effects of the Richardson number and Hartmann number arising from the MHD and Joule heating on the flow and heat transfer characteristics have been examined. The results show that the flow behavior, temperature distribution and heat transfer inside the cavity are strongly affected by the presence of the magnetic field. On the other hand, only the temperature distribution and heat transfer inside the cavity are strongly affected by the Joule heating parameter. The results also show that if the Hartmann number is increased from 5 to 100 then the heat transfer detraction is 20%, and if the Joule heating parameter is increased from 1 to 5 then the heat transfer detraction is 58%. In addition, multiple regressions among the various parameters are obtained.

Index Terms: mixed convection, finite element method, lid-driven cavity, circular hollow plate, heat transfer detraction

1. Introduction

Mixed convection in a closed enclosure is a topic that has been studied extensively by researchers, especially those concerned with lid-driven cavity problems. This is because the topic has many applications in engineering and natural phenomena such as solar energy storage, growth of crystals, heat exchangers, cooling of electronic devices, food processing, atmospheric flows and drying technologies[1-5]. There are many research papers concerned with mixed convection in a lid-driven cavity, and some of them are described in what follows. Oztop and Dagtekin[6] numerically investigated mixed convection in a two-sided lid-driven differentially heated square enclosure. Moallemi and Jang[7] carried out a numerical investigation on the effects of Prandtl number on laminar mixed convection in a lid-driven cavity. Prasad and Koseff[8] experimentally investigated mixed convection in a deep lid-driven cavity. Khanafer and Chamkha[9] analyzed mixed convection in a lid-driven cavity that is filled with a fluid-saturated porous medium. Ji et al.[10] conducted a numerical and experimental investigation of mixed convection in a sliding lid-driven cavity. Sharif[11] studied mixed convection in shallow inclined driven enclosure with a top-heated moving lid and cooled from below. Oztop et al.[12] investigated mixed convection in lid-driven cavities with a solid vertical partition. Basak et al.[13] investigated mixed convection between linearly heated side walls in a lid-driven porous

Nomenclature

B_0	magnetic induction ()	V	dimensionless vertical velocity component
c_p	specific heat (J kg^{-1} k^{-1})	V_0	lid velocity(ms^{-1})
D	diameter of the inner plate	x	horizontal coordinate (m)
g	gravitational acceleration (ms^{-2})	X	dimensionless horizontal coordinate
Gr	Grashof number	y	vertical coordinate (m)
H	enclosure height (m)	Y	dimensionless vertical coordinate
Ha	Hartmann number		
k	thermal conductivity (Wm^{-1} k^{-1})	*Greek symbols*	
K	solid fluid thermal conductivity ratio	α	thermal diffusivity (m^2s^{-1})
J	Joule heating parameter	β	thermal expansion coefficient (K^{-1})
L	length of the enclosure (m)	μ	dynamic viscosity (kg m^{-1} s^{-1})
Nu	Nusselt number	ν	kinematic viscosity (m^2 s^{-1})
p	dimensional pressure (kg m^{-1} s^{-2})	θ	non-dimensional temperature
P	dimensionless pressure	ψ	streamfunction
Pr	Prandtl number	ρ	fluid density (kg m^{-3})
Re	Reynolds number	*Subscripts*	
Ri	Richardson number	av	average
T	fluid temperature (K)	h	heat source
u	horizontal velocity component (ms^{-1})	c	cold
U	dimensionless horizontal velocity component	f	fluid
v	vertical velocity component (ms^{-1})	s	solid

square enclosure. Sivasankaran et al.[14] performed a numerical investigation of mixed convection in a lid-driven enclosure with non-uniform heating on both sidewalls. Kalteh et al.[15] carried out a numerical investigation of steady laminar mixed convection in a nanofluid-filled lid-driven square enclosure with a triangular heat source. They revealed that the average Nusselt number can be increased by increasing the value of Reynolds number and decreasing the height of the heat source. Ismael et al.[16] numerically studied steady laminar mixed convection in a water-filled square enclosure. They observed that convection was reduced at the critical values obtained for the partial slip parameter. In addition, the partial slip parameter had an insignificant effect on convection in the enclosure.

Magneto-hydrodynamics (MHD) is nowadays an important field of study that is widely known for its usage in industrial applications such as metal casting, microelectronic devices, liquid metal cooling blankets for fusion reactors, turbulence control, crystal growth and heat and mass transfers control[4,17]. Some of the literature reviews concerned with MHD are as follows. Chamkha[1] performed a numerical investigation of hydromagnetic mixed convection with internal heat generation or absorption in a vertical lid-driven enclosure. Al-Salem et al.[4] numerically studied the effects of the moving top wall direction on MHD mixed convection in a square enclosure with a linearly heated bottom wall. They found out that when the magnetic field is increased, it reduces the heat transfer and the flow

intensity inside the cavity. Ahmed et al.[5] performed a numerical investigation of laminar MHD mixed convection in an inclined lid-driven square enclosure with an opposing thermal buoyancy force and sinusoidal temperature distributions on both vertical walls. They observed that increasing the Hartmann number resulted in an increasing heat transfer rate along the heated walls as well. Piazza and Ciofalo[18] numerically investigated MHD natural convection in a liquid-metal filled cubic cavity. Sankar et al.[19] carried out an investigation of natural convection in the presence of a magnetic field in a vertical cylindrical annulus. Kahveci and Oztuna[20] performed an investigation of MHD natural convection in a cavity in the presence of a heated partition. Sarries et al.[21] conducted a numerical investigation of MHD free convection in a laterally and volumetrically heated square enclosure. Oztop et al.[22] numerically studied MHD buoyancy-induced flow in a non-isothermally heated square cavity. Rahman et al.[23] carried out a numerical investigation of the conjugate effect of Joule heating and MHD mixed convection in an obstructed lid-driven square enclosure. They found that the strength of the magnetic field determines the heat transfer and fluid flow in the enclosure. Rahman et al.[24] numerically investigated the conjugate effect of Joule heating and MHD on double-diffusive mixed convection in a horizontal channel with an open enclosure. They observed that the Hartmann number has a considerable effect on the streamlines, isothermal lines, concentration and density contours. In addition, increasing the Hartmann number resulted in a decrease in the average Nusselt number at the heat source. Oztop et al.[25] conducted a numerical investigation of MHD laminar mixed convection in a lid-driven square enclosure with a corner heater. They revealed that increasing the Hartmann number resulted in a decrease in the heat transfer. This means that the magnetic field is an important parameter that controls the heat transfer and fluid flow in the enclosure. Sivasankaran et al.[26] carried out a numerical study of the effects of the sinusoidal boundary temperatures at the sidewalls on mixed convection in a lid-driven square enclosure in the presence of a magnetic field. They observed that the presence of the magnetic field largely determined the heat transfer and fluid flow in the enclosure. Farid et al.[27] numerically investigated MHD mixed convection in a lid-driven enclosure with a heated circular hollow cylinder placed at the centre. They discovered that increasing the Hartmann number caused the velocity of the flow to decrease thus resulting in decreases in the heat transfer and fluid flow intensity as well. Rahman et al.[28] conducted a numerical study of MHD mixed convection in an open channel with a fully or partially heated square enclosure. Selimefendigil and Oztop[29] performed a numerical investigation of MHD mixed convection in a partially heated right-angled triangular cavity, with an insulated rotating cylinder and filled with Cu-water nanofluid. They observed that the magnetic field caused the convection heat transfer to slow down and increasing the Hartmann number caused both the total entropy generation and the local and averaged heat transfer to decrease. Selimefendigil and Oztop[30] numerically investigated MHD mixed convection in a lid-driven square cavity filled with nanofluid in a presence of a rotating cylinder. They found that the convective heat transfer and velocity field were slowed down by the magnetic field. Thus, increasing the Hartmann number caused the average heat transfer to decrease. In addition, the magnetic field acted as a parameter controlling the local heat transfer.

The Joule heating parameter has received a considerable amount of attention lately, in particular in relation to MHD problems. Rahman et al.[23] carried out a numerical investigation of the conjugate effect of Joule heating and MHD mixed convection in an obstructed lid-driven square enclosure. They discovered that the Joule heating parameter has considerable influence on the streamlines and isotherms. Rahman et al.[24] numerically investigated the conjugate effect of Joule heating and MHD on double-diffusive mixed convection in a horizontal channel with an open enclosure. They observed that the Joule heating parameter has an insignificant influence on the streamlines and concentration contours, but has considerable influence on the isotherms and density contours. Barletta and Celli[31] analyzed the

effects of Joule heating and viscous dissipation on MHD mixed convection in a vertical channel. Mao et al.[32] carried out an investigation of Joule heating in MHD flows in channels with thin conducting walls. Parvin and Hossain[33] studied the conjugate effect of Joule heating and a magnetic field on mixed convection in a lid-driven enclosure with an undulated bottom surface. Ray and Chatterjee[34] conducted a numerical investigation of MHD mixed convection in a horizontal lid-driven square enclosure with a circular solid object located at the centre and corner heaters with Joule heating. They found out that the Joule heating parameter only has a minor effect on the overall flow field inside the enclosure. Azad et al.[35] performed a numerical investigation of the effects of Joule heating on the magnetic field and mixed convection inside a channel along with a cavity. Their results indicated that a higher Joule heating parameter resulted in reduced heat transfer. In addition, enhancing the Joule heating parameter caused the exit temperature to increase. Raju et al.[36] investigated MHD convective flow through a porous medium in a horizontal channel with an insulated and impermeable bottom wall in the presence of viscous dissipation and Joule heating.

The main purpose of the present investigation is to examine the heat transfer detraction for conjugate effect of Joule heating and magneto-hydrodynamics on mixed convection in a lid-driven cavity along with a heated circular plate placed at the centre of the square enclosure for different values of the Hartmann number, Richardson number and Joule heating parameter.

2. Problem Formulation

2.1. Physical Modeling

Figure 1 shows the computational domain of the enclosure considered in the study and the associated coordinate system. Here L and H represent the width and height of the enclosure respectively. The aspect ratio of the length to its height of the enclosure is unity, representing a square enclosure. In addition, D represents the diameter of the inner plate (D = 0.2L) and it is located at the center of the enclosure. The hollow plate is kept at a constant high temperature T_h. The vertical walls of the enclosure are kept in a constant low temperature T_c, while the horizontal walls are adiabatic. The right vertical wall of the enclosure is moving upwards with constant velocity V_0 in its own plane. A uniform magnetic field with constant magnitude B_0 is applied horizontally, normal to the y-axis. Joule heating is also applied to the enclosure. The radiation, pressure work and viscous dissipation are all negligible. A no-slip boundary condition is imposed on all the walls of the enclosure and the plate surface.

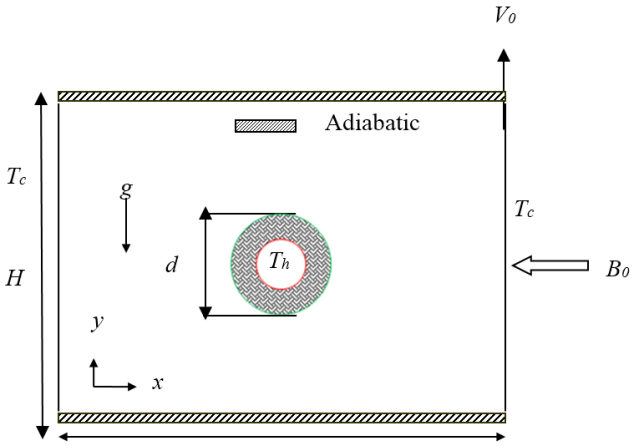

Figure 1. Schematic diagram of the physical model

2.2. Mathematical Formulation

With the following dimensionless variables:

$$X = \frac{x}{L},\ Y = \frac{y}{L},\ U = \frac{u}{V_0},\ P = \frac{p}{\rho {V_0}^2},$$
$$\theta = \frac{(T-T_c)}{(T_h-T_c)},\ \theta_s = \frac{(T_s-T_c)}{(T_h-T_c)}$$

the dimensionless forms of the governing equations for laminar, steady mixed convection based on the standard laws of conservation of mass, momentum and energy in the presence of hydromagnetic effects and Joule heating are given as:

$$\frac{\partial U}{\partial X} + \frac{\partial V}{\partial Y} = 0 \quad (1)$$

$$U\frac{\partial U}{\partial X} + V\frac{\partial U}{\partial Y} = -\frac{\partial P}{\partial X} + \frac{1}{Re}\left(\frac{\partial^2 U}{\partial X^2} + \frac{\partial^2 U}{\partial Y^2}\right) \quad (2)$$

$$U\frac{\partial V}{\partial X} + V\frac{\partial V}{\partial Y} = -\frac{\partial P}{\partial Y} + \frac{1}{Re}\left(\frac{\partial^2 V}{\partial X^2} + \frac{\partial^2 V}{\partial Y^2}\right) + Ri\,\theta - \frac{Ha^2}{Re}V \quad (3)$$

$$U\frac{\partial \theta}{\partial X} + V\frac{\partial \theta}{\partial Y} = \frac{1}{Re\,Pr}\left(\frac{\partial^2 \theta}{\partial X^2} + \frac{\partial^2 \theta}{\partial Y^2}\right) + J V^2 \quad (4)$$

For the solid region: $\frac{\partial^2\theta_s}{\partial X^2}+\frac{\partial^2\theta_s}{\partial Y^2}=0$ (5)

where

$Re=V_0L/\upsilon, Gr=g\beta\Delta TL^3/\upsilon^2,\ Ha^2=\sigma B_0^2L^2/\mu,$

$Pr=\nu/\alpha, Ri=Gr/Re^2, J=\sigma B_0^2LV_0/\rho C_p\Delta T$

(here $\Delta T=T_h-T_c$ and $\alpha=k/\rho C_p$ are the temperature difference and thermal diffusivity respectively) are the Reynolds number, Grashof number, Hartmann number, Prandtl number, Richardson number, and Joule heating parameter respectively.

The dimensionless boundary conditions for the problem under consideration can be written as follows:

At the left wall: $U=0, V=0,\ \theta=0$

At the right vertical wall: $U=0, V=1,\ \theta=0$

At the top and bottom walls: $U=0,\ V=0,\ \frac{\partial\theta}{\partial N}=0$

At the inner surface of the hollow cylinder: $U=0, V=0, \theta=1$

At the outer surface of the hollow cylinder: $\left(\frac{\partial\theta}{\partial N}\right)_{fluid}=K\left(\frac{\partial\theta_s}{\partial N}\right)_{solid}$

where N is the non-dimensional distance in either the X or Y direction acting normal to the surface, and $K = k_s/k_f$ is the thermal conductivity ratio.

The average Nusselt number at the heated hollow cylinder in the cavity, based on the conduction contribution, may be expressed as

$$Nu_{av}=-\frac{2}{\pi}\int_0^{\pi}\frac{\partial\theta}{\partial N}d\phi$$

And the average temperature in the cavity is defined as $\theta_{av}=\int\theta\, d\overline{V}/\overline{V}$, where $\overline{V}$ is the cavity volume.

The fluid motion is displayed using the stream function (ψ) obtained from velocity components U and V. The relationship between the stream function and the velocity components for a two-dimensional flow can be expressed as:

$$U=\frac{\partial\psi}{\partial Y},\ V=-\frac{\partial\psi}{\partial X} \quad (6)$$

3. Numerical Scheme

3.1. Numerical Procedure

The solutions of the governing equations along with boundary conditions are solved through the Galerkin finite-element formulation[24]. The continuum domain is divided into a set of non-overlapping regions called elements. Six node triangular elements with quadratic interpolation functions for velocity as well as temperature and linear interpolation functions for pressure are utilized to discretize the physical domain. Moreover, interpolation functions in terms of local normalized element coordinates are employed to approximate the dependent variables within each element. Substitution of the obtained approximations into the system of the governing equations and boundary conditions yields a residual for each of the conservation equations. These residuals are reduced to zero in a weighted sense over each element volume using the Galerkin method. The resultant finite-element equations are nonlinear. These nonlinear algebraic equations are solved employing the Newton-Raphson iteration technique.

3.2. Grid Independency Test and Code Validation

To establish the appropriate grid size, several grid size sensitivity tests were conducted in this geometry to determine the sufficiency of the mesh scheme and to make sure that the solutions are grid independent. The grid independent test are conducted for *Ri* = 1, *Ha* = 10 and *J* = 0.5 in the square lid-driven enclosure. Five different non-uniform grid systems with the following numbers of elements within the resolution field – 4032, 5794, 6116, 7270 and 8599 – are examined. In order to develop an understanding of the effects of the grid fineness, the average Nusselt number was calculated for each grid system as shown in ***Figure 2***. The size of Nu_{av} for 8599 elements shows little difference from the results obtained for the other elements. However, the grid independency test showed that a grid of 8599 elements is enough for the desired accuracy of the results.

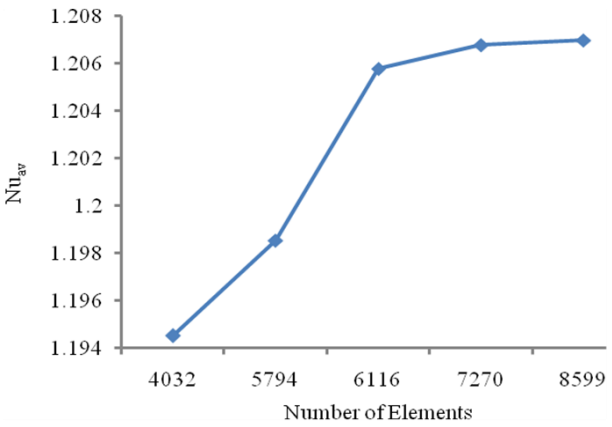

Figure 2. Grid independency study for average Nusselt number with *Ha* = 10, *J* = 0.5 and *Ri* = 1.

Table 1. Comparison of the present data with of Chamkha[1] for *Ha*

Parameter	Present study	Chamkha[1]
Ha	Nu	Nu
0.0	2.206915	2.2692
10.0	2.113196	2.1050
20.0	1.820612	1.6472
50.0	1.18616	0.9164

To verify the accuracy of the numerical results and the validity of the mathematical model obtained in the present study, comparisons with the previously published results are necessary. But owing to the lack of availability of experimental data on the particular problem with its associated boundary conditions investigated here, validation of the predictions could not be done against experiment. However, the present numerical model can be compared with the documented numerical study of Chamkha[1]. The present numerical code was validated against the problem of mixed convection in a lid-driven enclosure studied by Chamkha[1], which was investigated using a finite volume approach. The left wall moved upward with a fixed velocity and maintained in a cooled state. The right wall was heated whereas the two horizontal walls are adiabatic. We use the same boundary condition and wall temperatures on the horizontal walls of the cavity. We compared the results for average Nusselt number (at the hot wall) between the outcomes of the present code as shown in ***Table 1***. From the comparison it can be observed that the results of present simulation agree well with the results of Chamkha[1].

4. Results and Discussion

In this paper, a numerical investigation has been carried out to study the conjugate effect of Joule heating and magneto hydrodynamics on mixed convection in a lid-driven square cavity along with a heated hollow plate. The governing parameters used are the Hartmann number ranging from $5 \leq Ha \leq 100$, the Richardson number ranging from $0.1 \leq Ri \leq 5$ and the Joule heating parameter ranging from $1 \leq J \leq 5$. The Reynolds number, the solid fluid thermal conductivity ratio and the Prandtl number are fixed at *Re* = 100, *K* = 5 and Pr = 0.71. The numerical results are shown in the forms of streamlines, isotherms, average Nusselt number and average fluid temperature.

4.1. Effects of the Hartmann number

Figure 3 shows the effect of the Hartmann number on streamlines for *J* = 0.5 at different values of the Richardson number. In the forced convection dominated region at *Ri* = 0.1 and pure mixed convection dominated region at *Ri* = 1, the flow pattern and the flow strength are almost similar for all *Ha* values. In the forced and pure mixed convection dominated region for lower *Ha* values (= 5 and 20), a counter rotating cell appeared at the right corner which is generated by the moving right wall and as *Ha* increases to 50, the cell divided into two parts at which the cells then located near the top and bottom corner of the right wall. Both cells rotate in the same direction and have equal flow strength. When the *Ha* value increases to 100, the flow strength of the two cells decreases slightly from 0.02 to 0.01 in both forced and pure mixed convection dominated region. In the free convection dominated region at *Ri* = 5, the flow pattern changes dramatically for all *Ha* values. For the highest *Ha* value (*Ha* = 100), the two cells located at the right wall disappeared and four new cells are formed at the centre. All four cells rotate in the same direction. As *Ha* decreases to 50, two of the cells disappeared. The other two

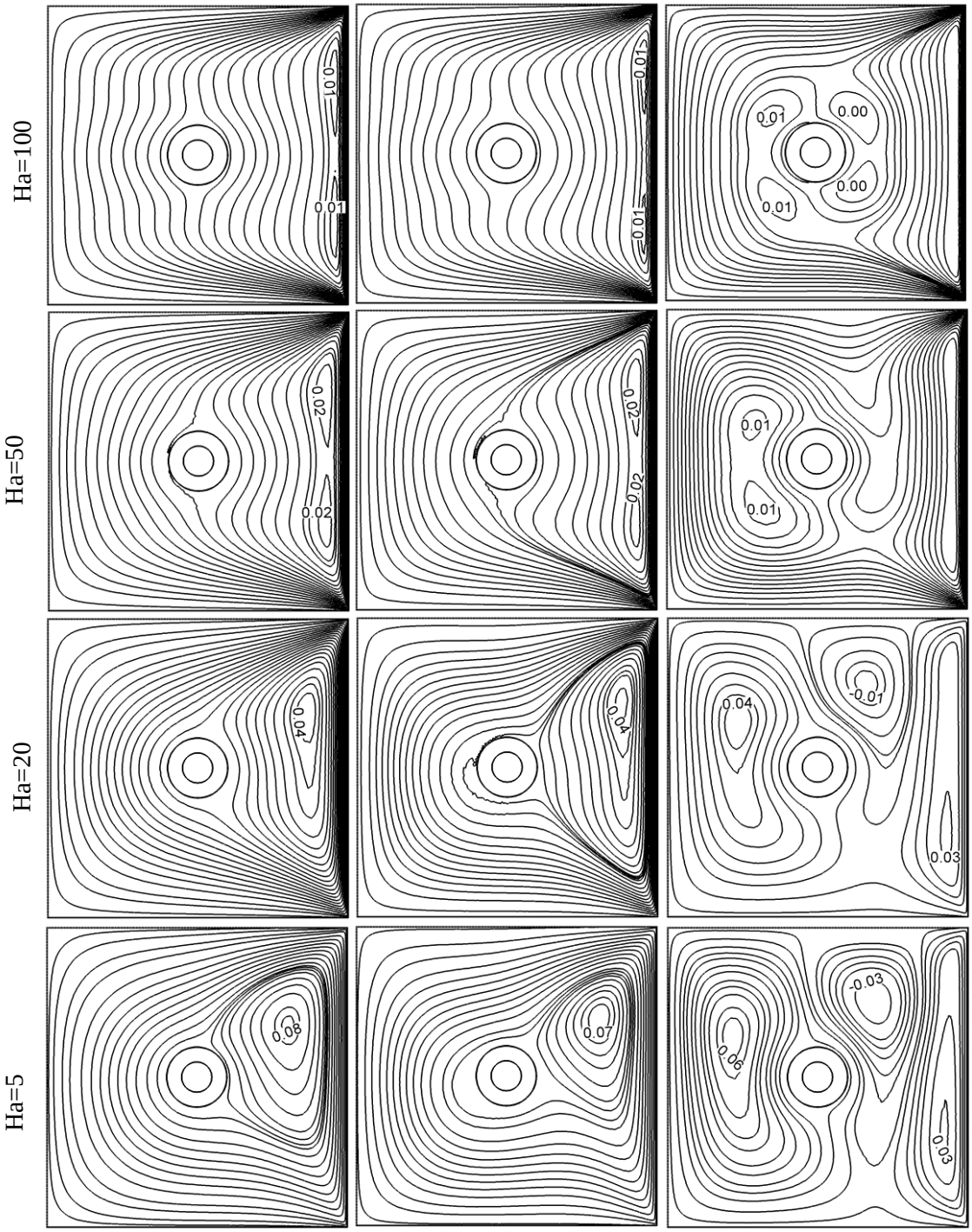

Figure 3. Effects of Hartman number and Richardson number on streamlines for $J = 0.5$.

cells which rotate counter clockwise remains at the centre near the left wall with equal flow strength. As *Ha* decreases to 20, multiple cells are formed. The two cells merge into one big cell which rotates counter clockwise and it is located near the left wall. Meanwhile, one cell is formed near the bottom corner of right wall which rotates counter clockwise and another cell is formed near the top right corner which rotates clockwise. At the lowest *Ha* value ($Ha = 5$), the pattern is more or less the same but with slightly higher flow strength.

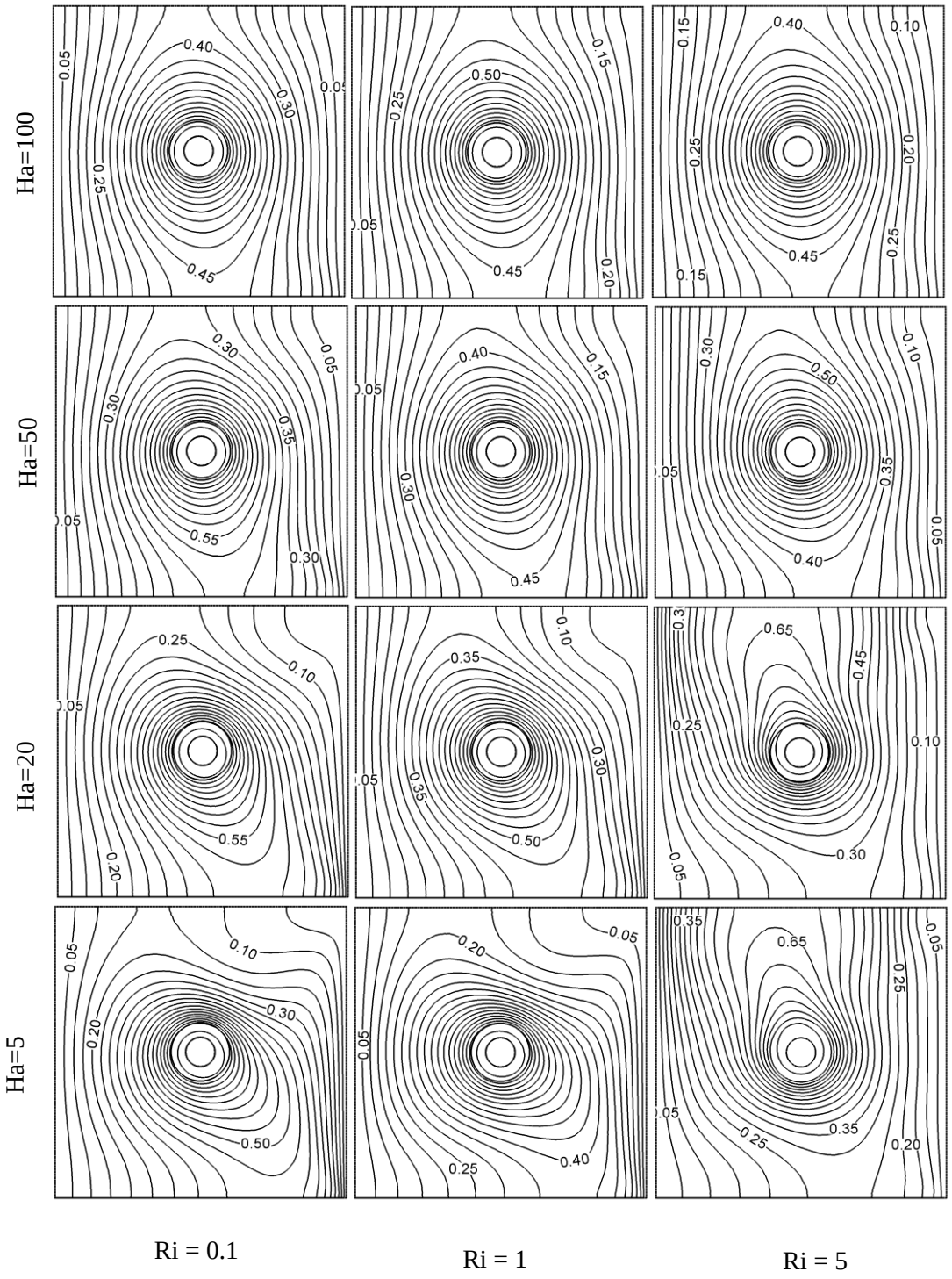

Figure 4. Effects of Hartman number and Richardson number on isothermal lines for $J = 0.5$.

The effect of Hartmann number on isotherms for $J = 0.5$ at different values of Richardson number is shown in ***Figure 4***. When $Ha = 50$ and 100, it can be seen that the isothermal lines is almost parallel to the vertical walls for all Ri values. This means that conduction heat transfer is the most active here. The isothermal lines near the vertical walls are almost similar at $Ri = 0.1$ and 1 for lower values of Ha (= 5 and 20) where convective distortion of isothermal lines takes place. Meanwhile for $Ri = 5$, although the isothermal lines are almost parallel to the vertical walls for higher Ha values (= 50 and 100), the isotherms changes as Ha decreases. The isothermal lines are

accumulated towards the upper left wall for lower *Ha* values (= 5 and 20) indicating a dominant influence of the convective heat transfer at *Ri* = 5. Another interesting change in the isotherms is found with the increase of the Hartmann number around the plate.

The effects of the Hartmann number on the average Nusselt number (Nu_{av}) at the hot surface with the Richardson number is presented in ***Figure 5***. The average Nusselt number at first decreases as the *Ri* value increases in the forced convection dominated region for lower *Ha* values (= 5, 20 and 50), then around *Ri* = 2 it starts to increase slowly for *Ha* = 20 and 50 and very rapidly for *Ha* = 5. But for *Ha* = 100, the average Nusselt number keeps decreasing steadily as *Ri* increases. In addition, the highest average Nusselt number is achieved at the lowest *Ha* value (= 5).

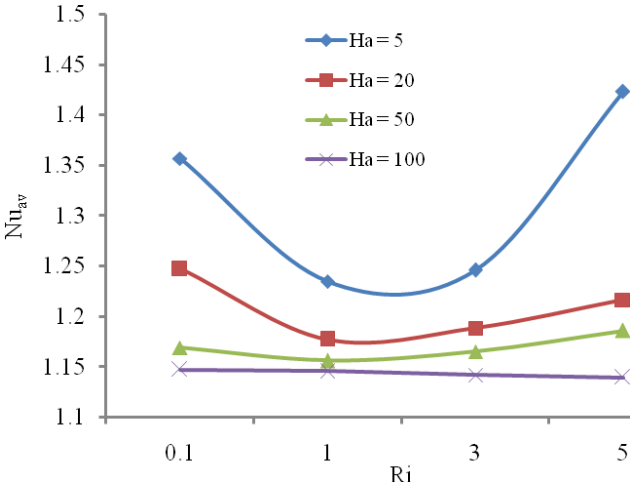

Figure 5. Effects of Hartman number and Richardson number on average Nusselt number for *J* = 0.5.

The effects of the Hartmann number on the average fluid temperature (θ_{av}) in the square enclosure with the Richardson number is presented in ***Figure 6***. For *Ha* = 20 and 50, the average fluid temperature is almost constant in the forced convection dominated region with increasing *Ri* but in the natural convection dominated region , it increases slowly with increasing *Ri* and as it reaches *Ri* = 3, it starts to increase quickly. Meanwhile for *Ha* = 5, the average fluid temperature initially decrease in the forced convection dominated region as *Ri* increases but at *Ri* = 1, it starts to goes up rapidly with increasing *Ri*. For *Ha* = 100, as *Ri* increases, the average fluid temperature is unstable as it keeps increasing then decreasing at some point before it starts to increase again. In addition, the following multiple regression for the average Nusselt number in terms of the Richardson number and the Hartmann number was obtained:

$$Nu_{av} = 0.0047Ri - 0.0014Ha + 1.2641$$

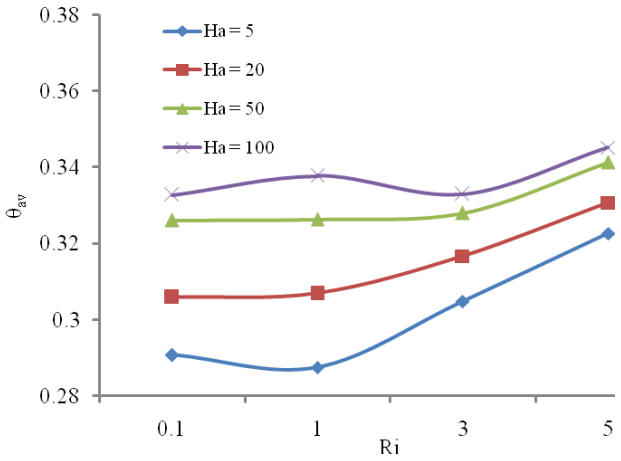

Figure 6. Effects of Hartman number and Richardson number on average fluid temperature for *J* = 0.5.

4.2. Effect of the Joule heating parameter

The effect of the Joule heating parameter on streamlines for *Ha* = 10 at different values of the Richardson number is shown in ***Figure 7***. In the forced convection dominated region at *Ri* = 0.1 and pure mixed convection dominated region at *Ri* = 1, a counter rotating cell appeared at the right corner which is generated by the moving right wall for different *J* values In the forced and pure mixed convection dominated region, the flow pattern and the flow strength are almost similar for all values of *J* except that the cell near the right wall becomes much smaller in size in the pure mixed convection dominated region compared to the forced-convection dominated region. In the natural-convection dominated region at *Ri* = 5 for *J* = 1, the flow pattern is distorted. The previous cell is pushed towards the right wall and two new cells are formed. One counter-rotating cell is formed near the left wall which is the largest cell and another cell is formed near the top right corner which rotates clockwise. The flow pattern does

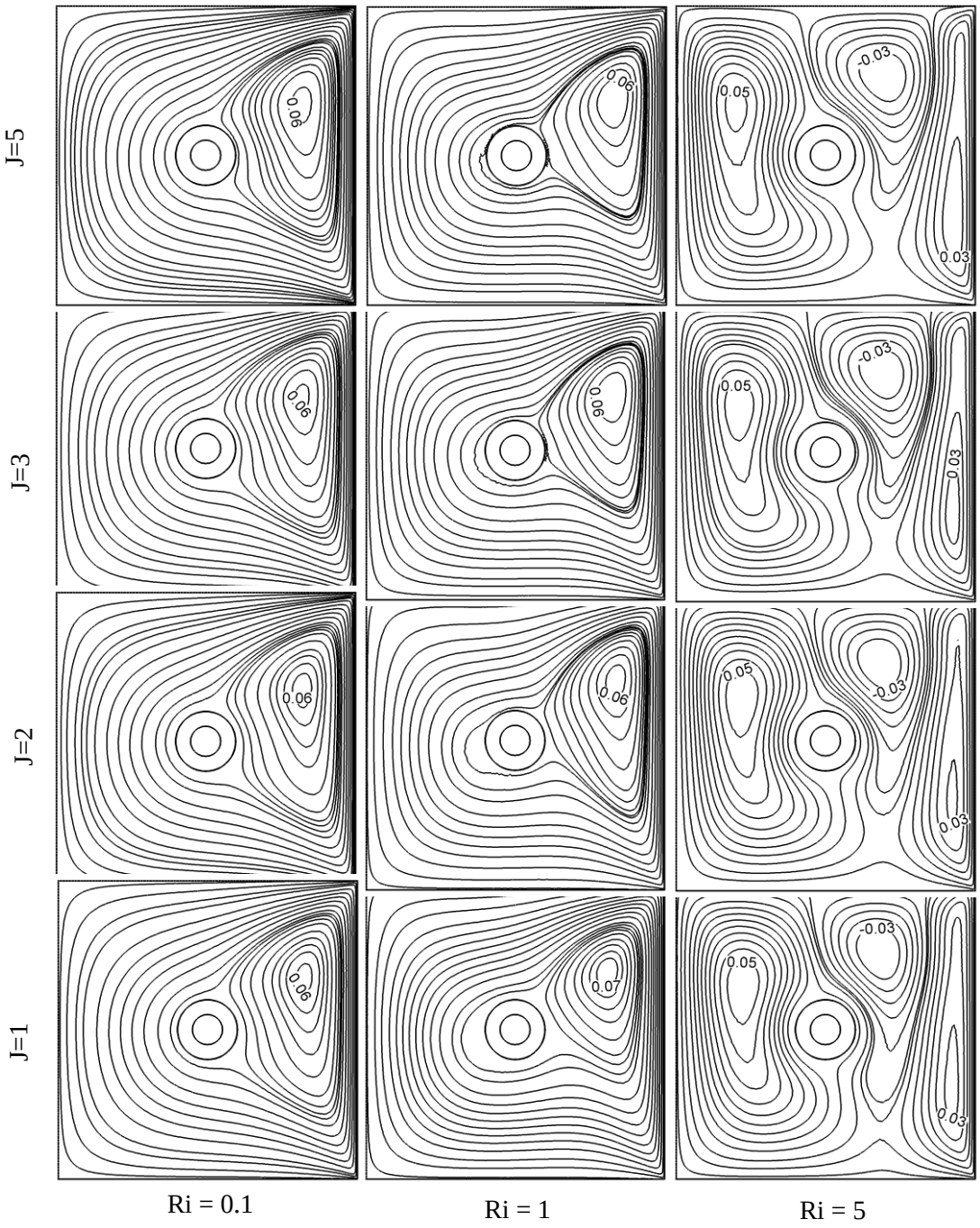

Figure 7. Effects of Joule heating parameter and Richardson number on streamlines for *Ha* = 10

not change much as the *J* values increase (*J* = 2, 3 and 5). Overall, this means that the Joule heating parameter has an insignificant effect on the streamlines.

Figure 8 shows the effect of Joule heating parameter on isotherms for *Ha* = 10 at different values of the Richardson number. In the forced convection dominated region at *Ri* = 0.1 for lower values of *J* (=1 and 2), the isothermal lines reveals a convective distortion pattern, while for higher *J* values (=3 and 5) it can be seen that the isothermal lines are almost parallel to the vertical walls which means conductive heat transfer is active. In the pure mixed-convection dominated region at *Ri* = 1 and *J* = 1, conductive distortion of the isothermal

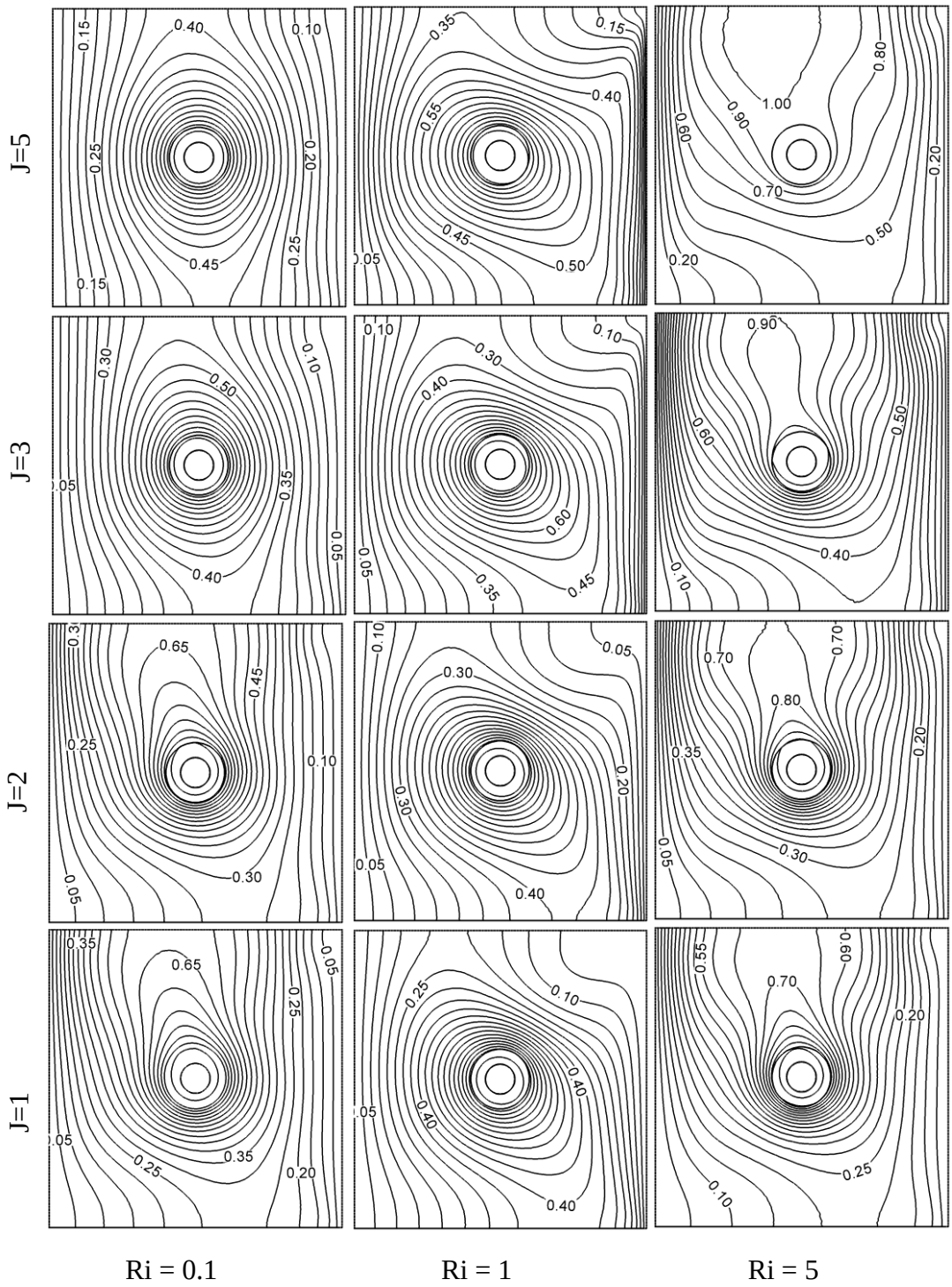

Figure 8: Effects of Joule heating parameter and Richardson number on isothermal lines for $Ha = 10$.

lines starts to appear near the top right corner. But it starts to disappear as the J values increase (for $J = 2$, 3 and 5) and the convective current becomes active. In the natural-convection dominated region at $Ri = 5$, the isothermal lines accumulate towards the upper left wall for all values of J, indicating the dominant influence of convective heat transfer.

The effects of the Joule heating parameter on the average Nusselt number (Nu_{av}) at the hot surface with the Richardson number are presented in

Figure 9. For higher *J* values (= 3 and 5), the average Nusselt number continuously decreases as *Ri* increases. On the other hand, the average Nusselt number initially decreases with increasing *Ri*, and when it reaches *Ri* = 3 it starts to go up faster for *J* = 1, but for *J* = 2 it increases more slowly. In addition, the highest average Nusselt number is achieved at the lowest *J* value (= 1) and the lowest average Nusselt number occurred at the highest *J* value (= 5).

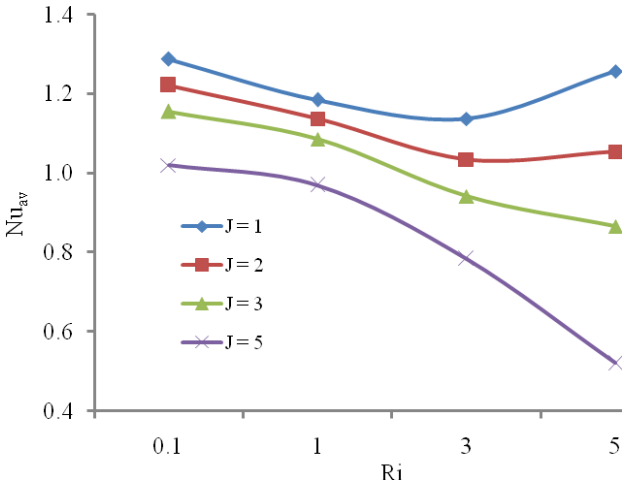

Figure 9. Effects of Joule heating parameters and Richardson number on average Nusselt number for *Ha* = 10

Figure 10 presents the effects of the Joule heating parameter on the average fluid temperature (θ_{av}) in the square enclosure with the Richardson number. The average fluid temperature decreases very slightly with increasing *Ri* for all *J* values in the forced-convection dominated region, whereas in the natural-convection dominated region it increases very rapidly with increasing *Ri* for all values of *J*. The highest average fluid temperature is obtained at the highest *J* value (= 5). In addition, the following multiple regression for the average Nusselt number in terms of the Richardson number and Joule heating parameter was obtained:

$$Nu_{av} = -0.0554Ri - 0.0999J + 1.4396$$

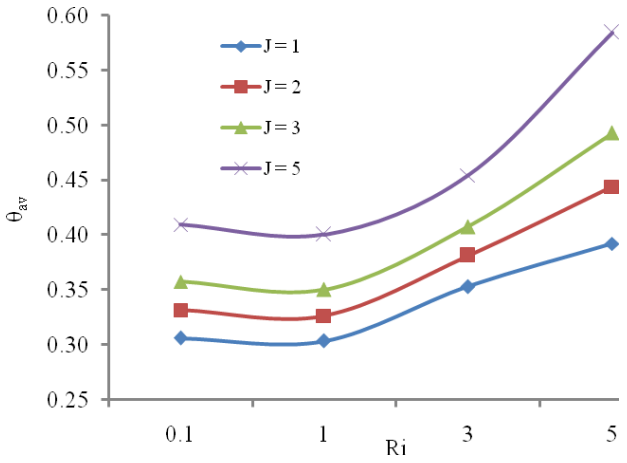

Figure 10. Effects of Joule heating parameters and Richardson number on average temperature for *Ha* = 10

5. Conclusion

MHD mixed convection in a lid-driven cavity with Joule heating and a heated hollow circular plate which is located at the centre of a square cavity has been numerically investigated over a wide ranges of various parameters such as the Hartmann number ($5 \leq Ha \leq 100$), Richardson number ($0.1 \leq Ri \leq 5$) and Joule heating parameter ($1 \leq J \leq 5$). From the investigation, the following conclusions can be made:

- The magnetic parameter (the Hartmann number) has a significant effect on reducing the size and strength of the inner vortex in the flow field for all values of *Ri*.
- A remarkable change in the isotherms around the plate is seen due as the Hartmann number increases for all *Ri*.
- The average Nusselt number declines and the average fluid temperature increases as the Hartmann number increases.
- The flow field is not influenced by the Joule heating parameter, but the isotherms near the plate are strongly influenced by *J* for all *Ri*.
- The average Nusselt number decreases and the average fluid temperature increases as the Joule heating parameter increases for all *Ri*.

References

[1] A. J. Chamkha, *Num. Heat Transfer*, **2002**, A 41, 529-546.

[2] U. Ghia, K. N. Ghia and C. T. Shin, *J. Comput. Phys.*, **1982**, 48, 387-411.

[3] M. C. Thompson and J. H. Ferziger, *J.Comput. Phys.*, **1989**, 82, 94-121.

[4] K. Al-Salem, H. F. Oztop, I. Pop and Y. Varol, *Int. J. Heat Mass Transfer*, **2002**, 55, 1103–1112.

[5] S. E. Ahmed, M. A. Mansour and A. Mahdy, *Nuclear Engineering Design*, **2013**, 265, 938-948.

[6] H. F. Oztop and I. Dagtekin, *Int. J. Heat Mass Transfer*, **2004**, 47, 1761-1769.

[7] M. K. Moallemi and K. S. Jang, *Int. J. Heat Mass Transfer*, **1992**, 35, 1881-1892.

[8] A. K. Prasad and J. R. Koseff, *Int. J. Heat Mass Fluid Flow*, **1996**, 17, 460-467.

[9] K. Khanafer and A. J. Chamkha, *Int. J. Heat Mass Transfer*, **1999**, 42, 2465-2481.

[10] T. H. Ji, S. Y. Kim and J. M. Hyun, *Int. J. Heat Mass Transfer*, **2007**, 43, 629-638.

[11] M.A.R. Sharif, *Appl. Therm. Eng.*, **2007**, 27, 1036-1042.

[12] H. F. Oztop, Z. Zhao and B. Yu, *Int. Comm. Heat Mass Transfer*, **2009**, 36, 661-668.

[13] T. Basak, S. Roy, S. K. Singh and I. Pop, *Int. J. Heat Mass Transfer*, **2010**, 53, 1819-1840.

[14] S. Sivasankaran, V. Sivakumar and P. Prakash, *Int. J. Heat Mass Transfer*, **2010**, 53, 4304-4315.

[15] M. Kalteh, K. Javaherdeh and T. Azarbarzin, *Powder Tech.*, **2014**, 253, 780-788.

[16] M. A. Ismael, I. Pop and A. J. Chamkha, *Int. J. Thermal Sciences*, **2014**, 82, 47-61.

[17] Z. Mehraz, A. E. Cafsi, A. Belghith and P. L. Quere, *J. Magnetism Magnetic Materials*, **2015**, 374, 214-224.

[18] I. D. Piazza and M. Ciofalo, *Int. J. Heat Mass Transfer*, **2002**, 45, 1477-1492.

[19] M. Sankar, M. Venkatachalappa and I. S. Shivakumara, *Int. J. Eng. Sci.*, **2006**, 44, 1556-1570.

[20] K. Kahveci and S. Oztuna, *Eur. J. Mech. B/Fluids*, **2009**, 28, 744-752.

[21] I. E. Sarries, S. C. Kakarantzas, A. P. Grecos and N. S. Vlachos, *Int. J. Heat Mass Transfer*, **2005**, 48, 3443-3453.

[22] H. F. Oztop, M. Oztop and Y. Varol, *Commun. Nonlinear Sci. Numer. Simul.*, **2009**, 14, 770-778.

[23] M. M. Rahman, M. A. Alim and M. M. A. Sarker, *Int. Comm. Heat Mass Transfer*, **2010**, 37, 524-534.

[24] M. M. Rahman, R. Saidur and N. A. Rahim, *Int. J. Heat Mass Transfer*, **2011**, 54, 3201-3213.

[25] H. F. Oztop, K. Al-Salem and I. Pop, *Int. J. Heat Mass Transfer*, **2011**, 54, 3494-3504.

[26] S. Sivasankaran, A. Malleswaran, J. Lee and P. Sundar, *Int. J. Heat Mass Transfer*, **2011**, 54, 512-525.

[27] S. K. Farid, M. M. Billah, M. M. Rahman and U. M. Sharif, *Procedia Eng.*, **2013**, 56, 474-479.

[28] M. M. Rahman, H. F. Oztop, R. Saidur, S. Mekhilef and K. Al-Salem, *Comp. Fluids*, **2013**, 79, 53-64.

[29] F. Selimefendigil and H. F. Oztop, *J. Taiwan Institute Chem. Eng.*, **2014**, 45, 2150-2162.

[30] F. Selimefendigil and H.F. Oztop, *Int. J. Heat Mass Transfer*, **2014**, 78, 741-754.

[31] A. Barletta and M. Celli, *Int. J. Heat Mass Transfer*, **2008**, 51, 6110-6117.

[32] J. Mao, S. Aleksandrova and S. Molokov, *Int. J. Heat Mass Transfer*, **2008**, 51, 4392-9.

[33] S. Parvin and N. F. Hossain, *J. Adv. Sci. Eng. Res.*, **2011**, 1, 210-23.

[34] S. Ray and D. Chatterjee, *Int. Comm. Heat Mass Transfer*, **2014**, 57, 200-207.

[35] A. K. Azad, M. M. Rahman and H. F. Oztop, *Procedia Eng.*, **2014**, 90, 389-396.

[36] K. V. S. Raju, T. S. Reddy, M. C. Raju, P. V. S. Narayana and S. Venkataramana, *Ain Shams Eng. J.*, **2014**, 5, 543-551.